


 Cite this: *Chem. Commun.*, 2021, 57, 8166

 Received 7th April 2021,
 Accepted 16th July 2021

DOI: 10.1039/d1cc01859k

rsc.li/chemcomm

An “AND”-logic-gate-based fluorescent probe with dual reactive sites for monitoring extracellular methylglyoxal level changes of activated macrophages†

 Wenli Wang,^{‡a} Junwei Chen,^{‡a} Huijuan Ma,^{‡a} Wanjin Xing,^a Nan Lv,^a Baoning Zhang,^a Huan Xu,^{*a} Wei Wang^{ib} ^{*ab} and Kaiyan Lou^{ib} ^{*a}

An “AND”-logic-gate-based fluorescent probe NAP-DCP-4 with dual reactive sites is reported, which has improved selectivity for methylglyoxal over glyoxal, featuring formaldehyde-enhanced methylglyoxal detection and irreversible and reversible turn-on fluorescence responses at different excitation wavelengths. Its cell-impermeability enables facile monitoring of extracellular methylglyoxal level changes in the supernatant of activated macrophages.

Methylglyoxal (MGO) is a highly reactive carbonyl species mainly formed in glycolysis from the degradation of glyceraldehyde-3-phosphate and dihydroxyacetone phosphate.^{1,2} MGO forms advanced glycation end products (AGEs) by glycating DNA, lipids, and proteins,³ causing protein dysfunctions,⁴ activation of RAGE receptor,² pro-inflammatory signaling and inflammation,^{5–8} and oxidative stress.^{9,10} Elevated MGO and AGE levels are observed in many diseases including diabetes,^{11–13} obesity,¹⁴ cancer,¹⁵ and Alzheimer's disease.¹⁶ Therefore, development of MGO probes for selective monitoring MGO levels is highly desirable.

In our lab, we are interested in MGO level changes of macrophages and their surrounding microenvironments upon activation. Macrophages are critical innate immune cells for host defence, immune surveillance of cancer cells and maintaining homeostasis.¹⁷ It is well known that macrophages can be activated by heterologous stimuli, such as lipopolysaccharide (LPS), through multiple intracellular pro-inflammatory signalling pathways, which shifts their metabolism from oxidative

phosphorylation to glycolysis to satisfy the elevated energy consumption.¹⁷ The increased glycolysis level leads to upregulated intracellular MGO levels resulting from both enhanced MGO production and decreased glyoxalase I (GLO1) expression, the key enzyme for MGO removal.^{18,19} While there were a few studies reported that intracellular MGO levels increase upon macrophage activation,^{18,19} extracellular MGO level changes and their potential contributions to inflammatory responses are not clear. It is possible that activated macrophages that excrete MGO would induce an extracellular MGO level increase in their microenvironment, which regulates physiological functions of the surrounding cells.²⁰ Although quite a few fluorescent probes have been reported for MGO detection (Fig. S1, ESI†), so far, there is no cell-impermeable probe available for monitoring the extracellular MGO level changes.

Herein, we would like to report the rational design of a cell-impermeable fluorescent probe **NAP-DCP-4** containing two polar reactive sites: an *o*-phenylenediamino (OPD) group and a guanidino (GND) group, forming an “AND” logic gate for the selective sensing of the extracellular MGO levels (Fig. 1 and Fig. S2, ESI†). Both reactive groups' reaction and sensing mechanism are well established in the literature. OPD is a fluorescence quenching group *via* a photo-induced electron transfer (PeT) mechanism.^{21–24} OPD-based fluorescent probes such as **PND-1** and **NP** react with MGO irreversibly to form methylquinoxalines, which interrupts the PeT quenching effect, resulting in a fluorescence turn-on response.^{22,23} Structurally similar glyoxal (GO) normally does not interfere with MGO detection in OPD-based probes because of its low reactivity.^{21,22,24} However, formaldehyde (FA) and nitric oxide (NO) may react with the OPD reactive group and interfere with MGO detection.^{21,25} In contrast, GND-based fluorescent probes **NAP-DCP-1** and **NAP-DCP-3** react with MGO or GO reversibly and show fluorescence turn-on responses *via* an intramolecular charge transfer (ICT) mechanism and excitation wavelength modulation to selectively excite the deprotonated adducts.²⁶ They show high selectivity over FA and NO, but cannot differentiate between MGO and GO with even higher fluorescence

^a State Key Laboratory of Bioengineering Reactor, Shanghai Key Laboratory of New Drug Design, and Shanghai Key Laboratory of Chemical Biology, School of Pharmacy, East China University of Science & Technology, 130 Meilong Road, Shanghai 200237, China. E-mail: xuhuan@ecust.edu.cn, kylou@ecust.edu.cn

^b Department of Pharmacology and Toxicology and BIO5 Institute, University of Arizona, Tucson, AZ 85721-0207, USA. E-mail: wwang@pharmacy.arizona.edu

† Electronic supplementary information (ESI) available: Experimental details, additional spectra, and ¹H NMR, ¹³C NMR and HRMS data. See DOI: 10.1039/d1cc01859k

‡ These authors contributed equally to this work.

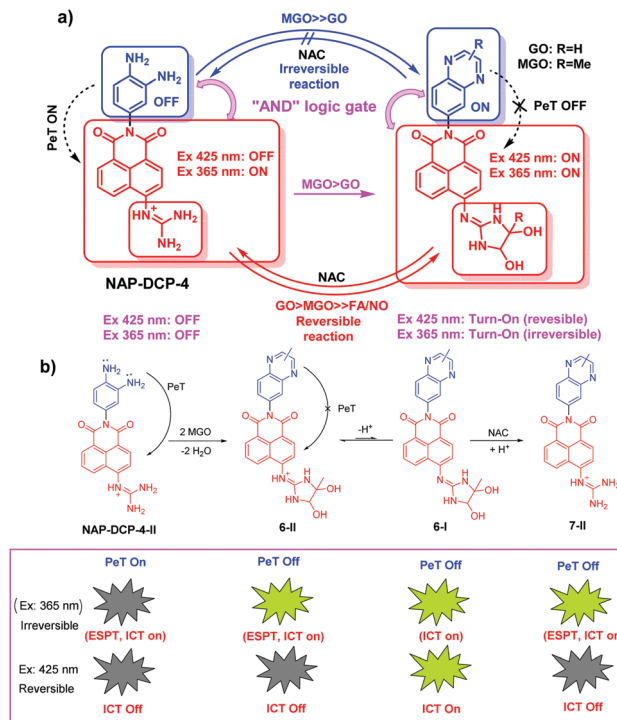


Fig. 1 (a) Probe design of **NAP-DCP-4**: an “AND”-logic-gate-based fluorescent probe with both OPD and GND reactive groups for improved MGO selectivity; (b) illustration of irreversible turn-on responses for MGO at $\lambda_{\text{ex}} = 365$ nm and reversible turn-on responses for MGO at $\lambda_{\text{ex}} = 425$ nm (only major species in equilibrium are shown).

turn-on ratio for GO.²⁶ We envisioned that incorporation of dual reactive groups, OPD and GND, into an “AND”-logic-gate-based probe would improve the GND-based probe’s selectivity for MGO over GO, while retaining high selectivity over FA and NO (Fig. 1a). We also envisioned that the incorporation of both reversible GND and irreversible OPD reactive groups may render the probe with both features of reversible ($\lambda_{\text{ex}} = 425$ nm, Off-On-Off) and irreversible ($\lambda_{\text{ex}} = 365$ nm, Off-On-On) fluorescence responses for reaction with MGO and then addition of *N*-acetyl cysteine (NAC), a known MGO quencher (Fig. 1b). Additionally, the combined use of the two polar reactive groups could possibly afford a cell-impermeable probe for monitoring extracellular MGO levels, as the calculated $\log P$ values from the molinspiration website²⁷ for **NP**,²³ **NAP-DCP-1**,²⁶ and **NAP-DCP-4** are 3.69, 1.69, and 1.19, respectively.

The probe **NAP-DCP-4** was conveniently synthesized from commercially available 4-bromo-1,8-naphthalic anhydride (**1**) in two steps in a 7.7% total yield and characterized by ¹H NMR, ¹³C NMR and HRMS (see ESI† Part II for more details).

We then studied the probe **NAP-DCP-4**’s *in vitro* fluorescence response for MGO in PBS buffer at pH 7.4. Similar to the GND-based probe **NAP-DCP-1**,²⁶ the UV-Vis spectra showed a red-shifted peak at 391 nm (Fig. S3, ESI†) due to the formation of the deprotonated dihydroxyimidazolidine adduct **6-II** with increased electron-donation at the 4-position of the 1, 8-naphthalimide (ICT On, Fig. 1b). When **6-II** was selectively excited at 425 nm, the “AND” effect of the “PeT Off” of the

methylquinoxaline formation (labelled in blue, Fig. 1b) and the “ICT On” of the dihydroxyimidazolidine formation (labelled in red, Fig. 1b) resulted in the fluorescence turn-on response for MGO (Fig. 2a). As expected, incorporation of the OPD group significantly reduced the probe’s turn-on response for GO (Fig. 2b). To estimate the contribution of the OPD group to the improvement of MGO selectivity over GO, the probe was excited at the isobestic absorption wavelength at 365 nm (see Fig. S3, ESI† for the isobestic point) to minimize the effect of the GND group’s reaction with MGO towards the fluorescence turn-on response. Under this excitation condition, both unreacted and reacted GND-substituted fluorophores (labelled in red in Fig. 1) have the same absorbance and are all emissive from either excited state proton transfer (ESPT) excited states (“ESPT, ICT on” for the protonated species in Fig. 1b) or excited state (“ICT on” for **6-I** in Fig. 1b) where there is no PeT quenching group attached.^{26,28} The fluorescence turn-on ratios

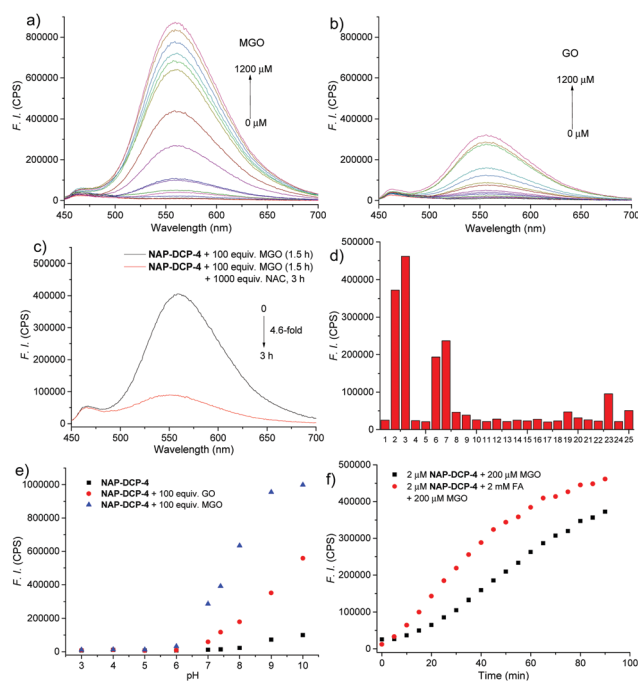


Fig. 2 (a and b) Fluorescence intensities of **NAP-DCP-4** (2 μM) upon addition of increased concentrations (0, 10, 20, 40, 60, 100, 150, 200, 300, 400, 500, 600, 800, 1000, and 1200 μM) of MGO (a) and GO (b) for 1.5 h; (c) fluorescence emission spectra of the probe **NAP-DCP-4** (2 μM) upon incubation with 100 equiv. MGO for 1.5 h versus further addition of 1000 equiv. NAC and then incubation for another 3 h; (d) fluorescence intensity at 559 nm of the probe **NAP-DCP-4** (2 μM) upon incubation with 100 equiv. of various other species. (1): probe only, (2): MGO, (3): MGO and 1000 equiv. FA, (4): FA, (5): acetaldehyde, (6): GO, (7): GO and 1000 equiv. FA, (8): *o*-phthalaldehyde, (9): glyoxylic acid, (10): benzaldehyde, (11) GSH, (12): glucose, (13): cysteine, (14): proline, (15): isoleucine, (16): H_2O_2 , (17): K^+ , (18): Na^+ , (19): Cu^{2+} , (20): Zn^{2+} , (21): Al^{3+} , (22): Ca^{2+} , (23): Fe^{2+} , (24): Fe^{3+} , (25) NOC-18; (e) pH-dependent fluorescence intensities at 559 nm of the probe **NAP-DCP-4** in response to 100 equiv. MGO or GO; (f) time-dependent fluorescence intensity increase of the probe **NAP-DCP-4** (2 μM) at 559 nm upon addition of 100 equiv. MGO with or without 1000 equiv. FA (all measurements were performed in 10 mM PBS buffer at 37 $^\circ\text{C}$, $\lambda_{\text{ex}} = 425$ nm).

were 24.7-fold for MGO *versus* 9.8-fold for GO (Fig. S4c and d, ESI†) under typical reaction conditions (2 μM probe incubated with 200 equiv. MGO or GO at pH 7.4 and 37 $^{\circ}\text{C}$ for 1.5 h), indicating that OPD indeed reacts much faster with MGO than with GO, which provides the basis for the improved selectivity for MGO over GO in **NAP-DCP-4**. Upon excitation with 425 nm light, the “AND”-logic-gate-based probe showed 21.2 and 11.1-fold for MGO and GO, respectively (Fig. S3a and b, ESI†). In contrast, the probe **NAP-DCP-1** bearing only the GND group had fluorescence turn-on ratios 11- and 19-fold for MGO and GO, respectively.²⁶

When excited at 425 nm, the probe's fluorescence turn-on response for MGO was reversible upon addition of NAC (Fig. 2c). The reversibility for GO was not as good as that of MGO, providing a further differentiation between MGO and GO (Fig. S6, ESI†). The probe has good selectivity for MGO (Fig. 2d) over many other reactive carbonyl species (FA, acetaldehyde, *o*-phthalaldehyde, glyoxylic acid, and benzaldehyde), GSH, glucose, amino acids (cysteine, proline, and isoleucine), H_2O_2 , metal ions (K^+ , Na^+ , Cu^{2+} , Zn^{2+} , Al^{3+} , Ca^{2+} , Fe^{2+} , and Fe^{3+}), and NO (from NOC-18, an NO donor). Further pH-dependence studies indicated that the probe is suitable for detection of MGO at pH higher than 6.0 (Fig. 2e).

Since FA may exist in biological systems at much higher concentration than MGO (up to 500 μM for FA²⁹ *versus* typical 1–4 μM for MGO²⁵) and often presents as an interfering species for MGO detection, we examined the potential effect of FA towards MGO detection by the probe **NAP-DCP-4**. When excited at 365 nm, no significant fluorescence intensity increase was observed for FA (Fig. S8, ESI,† column 4) compared with MGO (Fig. S8, ESI,† column 2), suggesting that FA reacts much slower with the OPD group than MGO under the same conditions. However, the coexistence of 10 times concentration of FA enhanced the probe's fluorescence turn-on response for MGO (Fig. 2d, columns 2 and 3), indicating that FA can compete with MGO to react with the OPD group and help the removal of its fluorescence quenching effect. When excited at 425 nm, time-dependent fluorescence intensity studies also confirmed FA-enhanced turn-on detection of MGO as a result of the “AND” logic gate (Fig. 2f). Accordingly, the limit of detection (LOD) for MGO improved from 2.2 μM to 1.8 μM in the presence of biologically relevant 400 μM FA (Fig. S7, ESI†). As a proof-of-concept study, the “AND”-logic-gate-based probe **NAP-DCP-4** turns an interfering specie (FA) into a promoting specie for the detection of the analyte of interest (MGO).

The potential interference of NO for MGO detection was also studied. UV-Vis studies showed that the presence of 1 mM NOC-18 seemed not to affect the formation of GND-MGO adducts at around 390 nm (Fig. S9a, ESI†). However, the fluorescence turn-on ratio for MGO in the presence of 1 mM NOC-18 was only 3-fold (Fig. S9b, ESI†). We propose that the formed benzotriazole between OPD and NO may deprotonate at pH 7.4, and function as a fluorescence quenching group *via* a PeT mechanism (Scheme S2, ESI†). Since the NO concentration is relatively low compared with those of FA and MGO in biological systems, its interference to MGO detection can be neglected.

From the above studies, the reaction and sensing mechanism was proposed in Fig. 1b based on the well-established reaction and sensing mechanism of each reactive group and formation of an “AND” logic gate (Fig. S2, ESI†). The proposed reaction mechanism was supported by HRMS studies that confirmed the formation of di-MGO adduct **6** (Fig. S11, ESI†) between the probe and excess amount of MGO and formation of the mono adduct **7** (Fig. S12, ESI†) when the reaction mixture was further treated with NAC. 3D fluorescence spectra also confirmed that the probe gives an irreversible turn-on response (Off–On–On, labelled as the red triangle) at $\lambda_{\text{ex/em}} = 365/559$ nm and reversible turn-on response (Off–On–Off, labelled as the green square) at $\lambda_{\text{ex/em}} = 425/559$ nm (Fig. S10, ESI†).

We further examined the probe's cell permeability and potential utility in sensing MGO level changes upon macrophage activation. RAW264.7 cells were selected as the model cell line, which were activated by lipopolysaccharide (LPS) stimulation (see ESI† part V for more details). In the cytotoxicity studies evaluated by MTS assay, the probe showed surprising nontoxicity up to 100 μM for both non-activated and activated RAW264.7 cells (Fig. S13, ESI†). Microplate readings of fluorescence intensity for both non-activated and activated RAW264.7 cells incubated with the probe (20 μM) did not show a statistically significant intensity increase compared with the control cells (Fig. S14, ESI†), indicating that the probe is cell impermeable. Otherwise, the probe-incubated cells should have shown enhanced fluorescence intensity compared with the control cells after the probe reacted with the intracellular MGO increasingly produced upon LPS activation. Further fluorescence imaging studies using cell-permeable **NAP-DCP-1** as the control also confirmed cell impermeability of the probe (Fig. S15, ESI†). We then took the cell culture supernatant for fluorescence analysis. When excited at 425 nm, RAW264.7 cells stimulated with LPS for 4 h had an apparent fluorescence intensity increase, which decreased upon addition of 5 mM NAC, confirming that the observed fluorescence increase was mostly due to increased MGO levels (Fig. 3a). Extended stimulation with LPS for 24 h resulted in further increase of fluorescence intensity, suggesting further elevated supernatant MGO level (Fig. 3b). A similar fluorescence intensity increase was observed

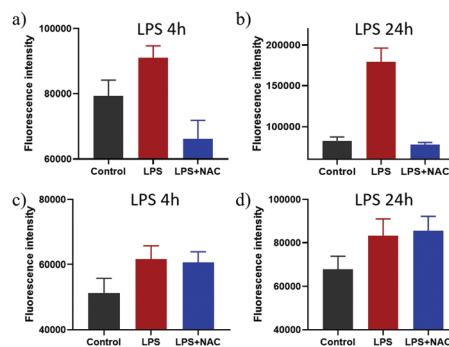


Fig. 3 Fluorescence intensity at 564 nm of **NAP-DCP-4** in the supernatant of RAW264.7 cells stimulated with LPS for 4 h (a and c) and 24 h (b and d): (a and b) $\lambda_{\text{ex}} = 425$ nm; (c and d) $\lambda_{\text{ex}} = 365$ nm.

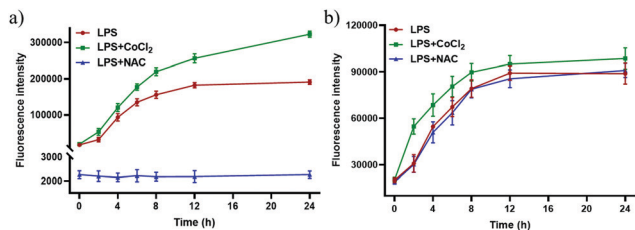


Fig. 4 Fluorescence intensities at 564 nm of **NAP-DCP-4** in the supernatant of RAW264.7 cells in normal or hypoxia microenvironments stimulated with LPS for 0, 2, 4, 8, 12, and 24 h: (a) $\lambda_{\text{ex}} = 425$ nm; (b) $\lambda_{\text{ex}} = 365$ nm.

upon LPS activation when excited at 365 nm, although it was not reversible upon addition of NAC (Fig. 3c and d). The above studies confirmed that the probe can be used to monitor the increase of supernatant MGO levels of macrophages upon activation.

We continued to study the probe's use for the monitoring of the supernatant MGO level changes of activated RAW264.7 cells under hypoxia conditions induced by CoCl_2 .³⁰ Time-dependent fluorescence intensity increases upon LPS stimulation were observed when excited with either 425 nm (Fig. 4a) or 365 nm (Fig. 4b) light. Upon addition of NAC, the fluorescence intensity increase remained almost unchanged when excited at 365 nm (Fig. 4b) in contrast to the fluorescence intensity dropping to low background values when excited at 425 nm (the blue curve in Fig. 4a), which confirmed MGO detection. It was also found that the fluorescence intensities measured were higher under hypoxia conditions at each time point, suggesting higher excreted MGO levels at hypoxia conditions due to further increased glycolysis for energy consumption. It was possible that the fluorescence intensity increase observed may partially come from increased FA concentrations. However, the increasing differences between the green curve under hypoxia conditions and the red curve under normal conditions when excited at 425 nm (Fig. 4a) compared with the rather unchanged fluorescence intensity differences when excited at 365 nm (Fig. 4b) still suggested more reacted GND group and higher MGO levels under hypoxia conditions.

In conclusion, we have reported an "AND"-logic-gate-based fluorescent probe **NAP-DCP-4** adopting two reactive sites: OPD and GND. The probe has improved selectivity for MGO over GO, featuring FA-enhanced MGO detection and unique irreversible and reversible fluorescence turn-on responses at two different excitation wavelengths. The potential utility of the probe for extracellular MGO detection was demonstrated in monitoring the MGO level changes in the supernatant of RAW264.7 cells upon LPS stimulation under either normal or hypoxia conditions.

The financial support by Shanghai Natural Science Fund (Grant No. 20ZR1414700), Shanghai Sailing Program (Grant No. 19YF1412500), the National Natural Science Foundation of China (Grant No. 21577037, 21738002, and 21906057) and the State Key Laboratory of Bioreactor Engineering is greatly appreciated.

Conflicts of interest

There are no conflicts to declare.

Notes and references

- M. P. Kalapos, *Toxicol. Lett.*, 1999, **110**, 145–175.
- N. Rabbani and P. J. Thornalley, *Amino Acids*, 2012, **42**, 1133–1142.
- P. J. Thornalley, *Gen. Pharmacol.*, 1996, **27**, 565–573.
- R. Singh, A. Barden, T. Mori and L. Beilin, *Diabetologia*, 2001, **44**, 129–146.
- D. Yao, T. Taguchi, T. Matsumura, R. Pestell, D. Edelstein, I. Giardino, G. Suske, N. Rabbani, P. J. Thornalley, V. P. Sarthy, H.-P. Hammes and M. Brownlee, *J. Biol. Chem.*, 2007, **282**, 31038–31045.
- H. Wang, Q. H. Meng, J. R. Gordon, H. Khandwala and L. Wu, *Clin. Biochem.*, 2007, **40**, 1232–1239.
- B. Vulesevic, B. McNeill, F. Giacco, K. Maeda, N. J. R. Blackburn, M. Brownlee, R. W. Milne and E. J. Suuronen, *Diabetes*, 2016, **65**, 1699–1713.
- C. Tikellis, R. J. Pickering, D. Tsorotes, O. Huet, M. E. Cooper, K. Jandeleit-Dahm and M. C. Thomas, *Diabetes*, 2014, **63**, 3915–3925.
- L. Wu and B. H. J. Juurlink, *Hypertension*, 2002, **39**, 809–814.
- N. Shangari, W. R. Bruce, R. Poon and P. J. O'Brien, *Biochem. Soc. Trans.*, 2003, **31**, 1390–1393.
- S.-Y. Goh and M. E. Cooper, *J. Clin. Endocrinol. Metab.*, 2008, **93**, 1143–1152.
- A. Prasad, P. Bekker and S. Tsimikas, *Curr. Cardiol. Rev.*, 2012, **20**, 177–183.
- A. K. Berner, O. Brouwers, R. Pringle, I. Klaassen, L. Colhoun, C. McVicar, S. Brockbank, J. W. Curry, T. Miyata, M. Brownlee, R. O. Schlingemann, C. Schalkwijk and A. W. Stitt, *Diabetologia*, 2012, **55**, 845–854.
- J. Masania, M. Malczewska-Malec, U. Razny, J. Goralska, A. Zdzienicka, B. Kiec-Wilk, A. Gruca, J. Stancel-Mozwillo, A. Dembinska-Kiec, N. Rabbani and P. J. Thornalley, *Glycoconjugate J.*, 2016, **33**, 581–589.
- D. Schroeter and A. Hoehn, *Curr. Pharm. Des.*, 2018, **24**, 5245–5251.
- C. Angeloni, L. Zamboni and S. Hrelia, *BioMed Res. Int.*, 2014, 238485.
- A. Viola, F. Munari, R. Sánchez-Rodríguez, T. Scolaro and A. Castagna, *Front. Immunol.*, 2019, **10**, 1462.
- T. Aki, T. Funakoshi, K. Noritake, K. Unuma and K. Uemura, *Sci. Rep.*, 2020, **10**, 10581.
- D. Prantner, S. Nallar, K. Richard, D. Spiegel, K. D. Collins and S. N. Vogel, *J. Leukocyte Biol.*, 2021, **109**, 605–619.
- T. Baumann, A. Dunkel, C. Schmid, S. Schmitt, M. Hiltensperger, K. Lohr, V. Laketa, S. Donakonda, U. Ahting, B. Lorenz-Depiereux, J. E. Heil, J. Schredelseker, L. Simeoni, C. Fecher, N. Körber, B. Bauer, N. Hüser, D. Hartmann, M. Laschinger, K. Eyerich, S. Eyerich, M. Anton, M. Streeter, T. Wang, B. Schraven, D. Spiegel, F. Assaad, T. Misgeld, H. Zischka, P. J. Murray, A. Heine, M. Heikenwälder, T. Korn, C. Dawid, T. Hofmann, P. A. Knolle and B. Höchst, *Nat. Immunol.*, 2020, **21**, 555–566.
- T. Wang, E. F. Douglass, Jr., K. J. Fitzgerald and D. A. Spiegel, *J. Am. Chem. Soc.*, 2013, **135**, 12429–12433.
- T. Tang, Y. Zhou, Y. Chen, M. Li, Y. Feng, C. Wang, S. Wang and X. Zhou, *Anal. Methods*, 2015, **7**, 2386–2390.
- S. Gao, Y. Tang and W. Lin, *J. Fluoresc.*, 2019, **29**, 155–163.
- M. Yang, J. Fan, J. Zhang, J. Du and X. Peng, *Chem. Sci.*, 2018, **9**, 6758–6764.
- F. Shaheen, A. Shmygol, N. Rabbani and P. J. Thornalley, *Biochem. Soc. Trans.*, 2014, **42**, 548–555.
- H. Xu, Q. Liu, X. Song, C. Wang, X. Wang, S. Ma, X. Wang, Y. Feng, X. Meng, X. Liu, W. Wang and K. Lou, *Anal. Chem.*, 2020, **92**, 13829–13838.
- <https://www.molinspiration.com/cgi-bin/properties>, 2021.
- J. Zhou, H. Liu, B. Jin, X. Liu, H. Fu and D. Shangguan, *J. Mater. Chem. C*, 2013, **1**, 4427–4436.
- K. J. Bruemmer, T. F. Brewer and C. J. Chang, *Curr. Opin. Chem. Biol.*, 2017, **39**, 17–23.
- J. Muñoz-Sánchez and M. E. Cháñez-Cárdenas, *J. Appl. Toxicol.*, 2019, **39**, 556–570.